Geomechanics and Engineering, *Vol. 28, No. 5 (2022) 531-546*
https://doi.org/10.12989/gae.2022.28.5.531

Investigation on ground displacements induced by excavation of overlapping twin shield tunnels

Weiqiang Qi[1], Zhiyong Yang*[1], Yusheng Jiang[1], Xing Yang[1], Xiaokang Shao[1] and Hongbin An[2]

[1]*School of Mechanics and Civil Engineering, China University of Mining and Technology-Beijinig, Ding, No. 11 Xueyuan Road, Haidian District, Beijing, 100083, P.R. China*
[2]*China Railway 12th Bureau Group Co., Ltd., No. 19 Renmin South Road, Xiaodian District, Taiyuan, Shanxi, 030000, P.R. China*

(Received January 25, 2021, Revised January 10, 2022, Accepted January 18, 2022)

Abstract. Ground displacements caused by the construction of overlapping twin shield tunnels with small turning radius are complex, especially under special geological conditions of construction. To investigate the ground displacements caused due to shield machines in the unique calcareous sand layers in Israel for the first time and determine the main factors affecting the ground displacements, field monitoring, laboratory geological analysis, theoretical calculations, and parameter studies were adopted. By using rod extensometers, inclinometers, total stations, and automatic segment-displacement monitors, subsurface tunneling-induced displacement, surface settlement, and displacement of the down-track tunnel segments caused by the construction of an up-track tunnel were analyzed. The up-track tunnel and the down-track tunnel pass through different stratum, resulting in different construction parameters and ground displacements. The laws of variation of thrust and torque, soil pressure in the chamber, excavated soil quantity, synchronous grouting pressure, and grout volume of the two tunnels from parallel to fully overlapping orientations were compared. The thrust and torque of the shield in the fine sand are larger than those in the Kurkar layer, and the grouting amount in fine sand is unstable. According to fuzzy statistics and Gaussian curve fitting of the shield tunneling speed, the tunneling speed in the Kurkar stratum is twice that in the fine-sand stratum.

Keywords: calcareous sand stratum; geological characteristics; ground displacement; parametric study; shield tunneling

1. Introduction

The steady expansion of cities has generated opportunities for the development of the urban rail transit systems worldwide. The shield tunneling method is extensively used in urban rail transit constructions owing to its unique advantages of strong adaptability, fast construction speed, safety, reliability, and small environmental impact. The double-track parallel layout is the main method used in the early design of the subway tunnel line. The spatial position of this layout is relatively simple, and the construction disturbances between the two railway lines is also small (Ocak 2013, Nawel and Salah 2015). To ensure the quality and safety of subway tunnel construction, engineers ensure that the turning radius of the subway line is relatively large. However, with the expansion of urban ground buildings and the continuous development of underground space, irregular utilization, and other factors, the route of the shield tunnel is subject to an increasing number of constraints, which makes the line type more complex (Yamaguchi *et al*. 1998, Sugimoto *et al*. 2007, Fang *et al*. 2020). Owing to the limitations of these factors, it is difficult to develop a subway line design. Therefore, the staggered and overlapped line design must be chosen instead. Following the advances in urban subway engineering and underground utility tunnel construction, an increasing number of overlapping shield tunnels with a small turning radius curve are being constructed. It is necessary to explore the ground displacement caused by the construction of overlapping shield tunnels with a small turning radius curve.

Based on the statistical analysis of the monitoring data of field surface settlement during the past few decades, researchers obtained the distribution of surface settlement in line with the Gaussian curve (Peck 1969). Subsequently, the numbers of research studies on the parameters relevant to surface subsidence have increased, and an increased number of curve prediction formulas suitable for specific strata have been fitted (Attewell and Woodman 1982, O'Reilly and New 1982, Mair *et al*. 1993, Celestino *et al*. 2000, Mollon *et al*. 2013, Liu *et al*. 2020). Rowe and Lee (1992) first proposed a functional expression for the parameters of tail shield clearance used to predict surface subsidence. Verruijt and Booker (1996) proposed a method to solve the displacement and stress of a tunnel face in a semi-infinite medium subject under the conditions of incompressible soil and elliptical tunnel face. Loganathan and Poulos (1998) redefined the "equivalent surface loss parameter" and applied it to the analytical solution of ground movement around clay tunnels. Ding *et al*. (2017) argued that the Gaussian curve or peck formula used for predicting the settlement under adjacent buildings caused by shield construction were unreasonable according to the actual

*Corresponding author, Ph.D.
E-mail: yangzy1010@126.com

ISSN: 2005-307X (Print), 2092-6219 (Online)

monitoring results. They proposed the characteristics of the surface settlement curve and the relevant calculation formulas when the tunnel was located under the building, within, and outside the disturbance range. Thus far, the soil displacement caused by the construction of twin tunnels in linear sections in the subway constructions in major cities in the world, such as London (Wan *et al*. 2017, Sugiyama *et al*. 1999), Madrid (Melis *et al*. 2002), Istanbul (Hasanpour *et al.* 2012), Washington (Nelson and Watry 2015), Rome (Miliziano and de Lillis 2019), Tabriz (Rezaei *et al*. 2019, Rezaei *et al*. 2020), Hague (Broere and Festa 2017), and others, has been extensively studied. The application of real-time field monitoring and numerical analysis makes the study of soil displacement caused by shield tunnel excavation more comprehensive (Karakus *et al*. 2007, Kim *et al*. 2018, Qi *et al*. 2021). Standing and Selemetas (2013) and Wan *et al*. (2017) used total stations, extensometers, and inclinometers to measure the ground settlement and horizontal and vertical displacement changes of the soil mass caused by a twin shield tunnel construction in clay stratum in London. Based on the subway tunnel project in Lyon, France, Dias and Kastner (2013) compared the horizontal and vertical displacements of the soil mass monitored *in situ* based on numerical analysis. The analysis considered the slurry pressure on the tunnel face, shield conicity, grouting pressure, and consolidation of grout in the shield excavation gap. Eskandari *et al*. (2018) used finite element software to study the relationship among earth pressure balance (EPB), surface settlement, and tunnel face displacement at the Mashhad Urban Railway Project in Iran. Kim *et al*. (2020) studied the effects of the parameters of shield construction on surface settlement based on the shield construction data of a soft soil layer in Hong Kong. These factors are a culmination of the effects of various other induced factors. Broere *et al*. (2017) and Festa *et al*. (2015) studied the correlation between the kinematic characteristics of the shield and the ground displacement based on the double-hole tunnel in Hague in the Netherlands. They revealed the physical principle of the interaction between shield machines and soil. In turn, Fang *et al*. (2020) used the Flac^{3D} numerical software to simulate the entire construction process of the fully overlapping shield tunnels of Tianjin Metro in China. The peck formula was modified according to the measured surface settlement, and the prediction formula of the surface settlement curve in the soft soil layer was then obtained.

An in-depth review of the literature showed that the research methods and achievements for ground displacement caused by the linear-line shield tunnel were relatively mature. However, the numbers of studies on the ground displacement caused by the construction of overlapping shield tunnels with small turning radius have been limited. Furthermore, contemporary research methods mainly use numerical simulations to study the excavation disturbance effects of curved shield tunnels. Additionally, few studies have systematically measured the horizontal and vertical displacements, and *in situ* segmental responses of deep soil for overlapping shield tunnels with a small turning radius curve. Based on the first subway tunnel constructed in Israel, this study analyzes the geological characteristics and the ground displacements in detail, thus providing a theoretical basis and an engineering reference to the shield construction control of the displacement of the stratum, shield machine parameter control, and shield type selection design for the calcareous sand layer of Israel. In this paper, Kurkar formation is more likely to cause larger settlement than fine-sand layer. The shield machine parameters in fine-sand layer are generally larger than those in Kurkar formation, while the tunneling speed in fine-sand layer is lower than that in Kurkar formation. Thus, research on the displacement of the deep stratum can provide a basis for the prediction of the influence of shield tunneling on underground as well as surrounding structures in Israel.

2. Field monitoring and geotechnical test

2.1 General information on tunnels

The Red Line light rail is the first urban underground railway in Tel Aviv, Israel, and the first subway tunnel constructed by using the shield method in the country. The eastern section of the Red Line light rail project is located in the center of the city, and has a total length of 6 km. The project is surrounded by densely packed buildings and heavy traffic. Many underground pipelines course below the project. The metro tunnel of the east section was constructed using two Herrenknecht EPB tunnel boring machines (TBMs) with diameters of 7.55 m. The shield was launched at the depot, passed through the EM Hamoshavot station and the Aharanovitz station, and finally arrived at Ben Gurion station. The line plan is illustrated in Fig. 1. In the section from EM Hamoshavot station to Geha interchange, the relative positions of lines 5 and 6 change from parallel to fully overlapped, and the overlapped clear distance is 4–6 m. The radius of the tunnel line in this section is 220 m, and it reduces to 190 m at approximately 40 m before the shield arrives. Line 6 is the down-track tunnel and line 5 the up-track one. After TBM1 completes the construction of line 6, TBM2 starts to complete line 5. The tunnel has an outer diameter of 7.2 m, an inner diameter of 6.5 m, a segment thickness of 350 mm, and segment ring widths of 1.5 m and 1.2 m in linear and curved sections, respectively.

2.2 Test setup and instruments

To analyze the influence of constructing overlapping shield tunnels on ground displacement and segment deformation in complex conditions, numerous field monitoring studies were conducted on the tunnel section with an overlap angle of 86°. The plane and profile of the monitoring instrument installation are shown in Fig. 2. Two inclinometers, C1 and C2, are set 3 m from the edge of both sides of the two tunnels to monitor the transverse and longitudinal horizontal displacements of the soil. The inclinometer was at a depth of 36 m, and readings were obtained every 0.5 m. Two extensometers with five anchors were installed at 3 m from the edge of both sides of the two tunnels, referred to as E1 and E3, respectively. An

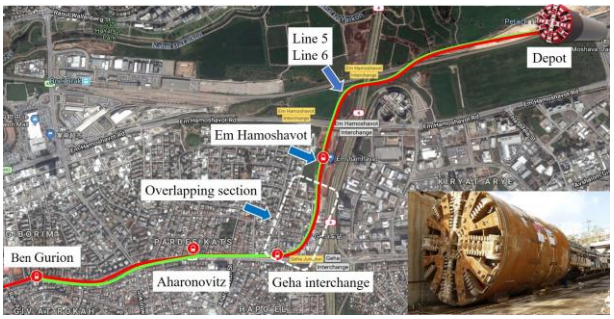

Fig. 1 Plan of east section of Red Line light rail project

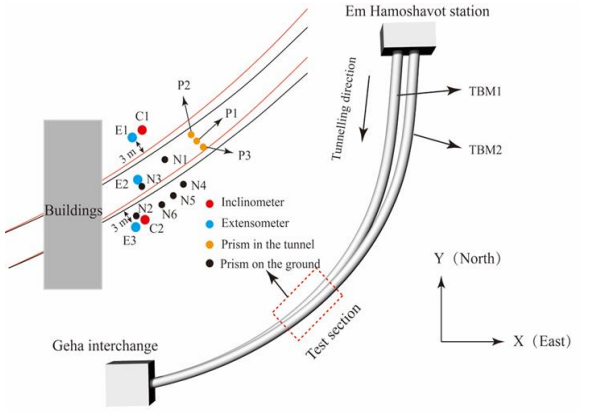

(a) Instrumentation layout plan

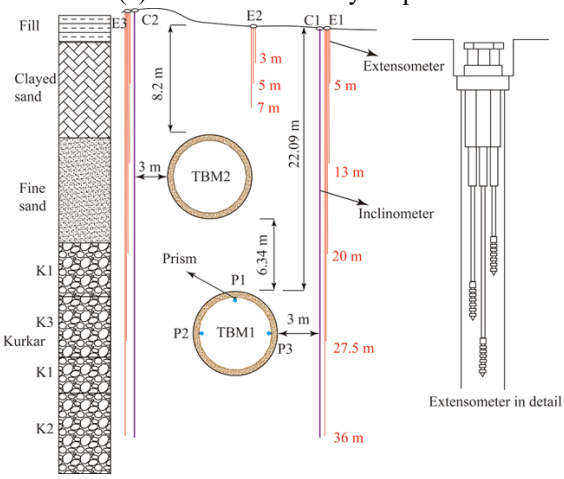

(b) Profile of monitoring points

Fig. 2 Layout of monitoring instruments

extensometer with three anchors was installed in the middle of the two tunnels and is referred to as E2. These extensometers were used to monitor the vertical displacement of soil at different depths. The five anchors of extensometers E1 and E3 were at depths of 5, 13, 20, 27.5, and 36 m, and the three anchors of the extensometer E2 were at depths of 3, 5, and 7 m, respectively. Six monitoring points, numbered N1–N6, were arranged on the surface to monitor the surface settlement. After constructing the down-track tunnel, three prisms were installed on the segments to monitor the impact of the construction of a shield for the up-track tunnel on the segment of the down-track tunnel. The field instrument installation is shown in Fig. 3.

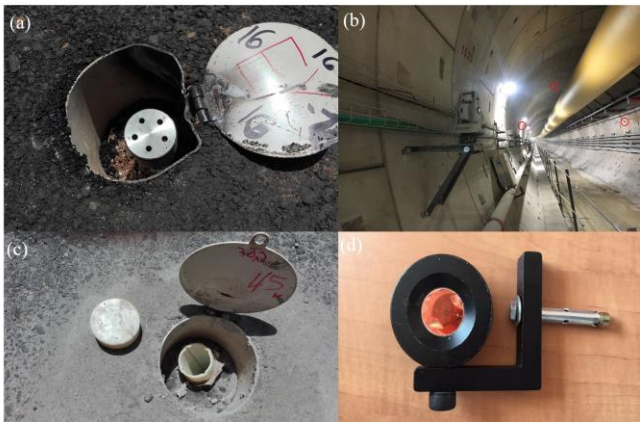

Fig. 3 Installation of field instruments: (a) Extensometer, (b) total station, (c) inclinometer, and (d) prism

Table 1 Description of surrounding rocks in Kurkar stratum

Ground type	Soil description
Kurkar (*K*1)	Sand, clean to calcareous, with 10–20% Kurkar gravel (diameter of 1–3 cm)
Kurkar (*K*2)	Alternate thin layer (1–2 cm thick) of clean loose sand interbedded with fragile Kurkar plates (thickness of 1–2 cm)
Kurkar (*K*3)	Alternate layers of solid, hard, rough surface laminar Kurkar sheets (thickness of 2–15 cm) interbedded with loose sand
Kurkar (*K*4)	Quasi-solid rock (saturated UCS 0.5–20 MPa), or nonconcretionary rock, solid throughout (saturated UCS > 20 MPa)

2.3 Geotechnical test

This section describes the shield passing through fine sand and Kurkar stratum, which is unique to Israel. The underground water level is approximately 13 to 14 m deep, and the down-track tunnel is below the water level. In fine sand, approximately 10% of the particles have diameters less than 0.1 mm, while 50–70% have a diameter less than 0.5 mm. Fine sand is composed of 70–80% quartz, and calcite is 20–30%. Kurkar is a type of weakly cemented, calcareous sand layer with high-quartz content and strong abrasiveness. The permeability coefficient of fine sand is as high as 5×10^{-4} m/s. The geological parameters of the Kurkar stratum are listed in Table 1. Fig. 4 shows the grain distribution curve of the Kurkar stratum. Other types of soil include sand, mixed grain soils, and clay. Frydman (2011) performed detailed *in-situ* and triaxial tests on Israel's unique geological characteristics, providing basic data for underground engineering, as shown in Table 2, and the geological profile and geological field photographs are shown in Fig. 5.

RoqSCAN technology was used to automatically analyze the mineral composition of the Kurkar samples. The results revealed calcite (40–60%), quartz (20–30%), and ankerite (10–20%) as the main constituents of Kurkar. The test results are illustrated in Figs. 6(a) and 6(b). Scanning electron microscopy shows that calcite with comb-like structure can be observed at the interface between the cement and the quartz sand. Quartz sand has

Table 2 Physical and mechanical parameters of the strata

Layer	γ_{sat} (kN/m)	k_0	C (kPa)	E (MPa)	φ (°)	h (m)
Fill	18.4	0.42	8	20	25	1.6
Clayed sand	20	0.36	10	35	20	7.2
Fine sand	19	0.3	0	50	35	8.4
Kurkar (*K*1)	19	0.34	30	70	35	3.7
Kurkar (*K*3)	21	0.36	40	90	38	4.1
Kurkar (*K*1)	19	0.34	30	70	35	3.8
Kurkar (*K*2)	20	0.34	36	80	36	2.7

Note: γ_{sat} = soil saturated unit weight; k_0 = lateral pressure coefficient; C = cohesion; E= elastic modulus; φ = friction angle; h = thickness

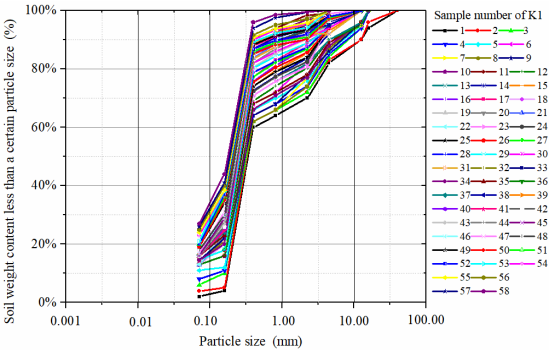

(a) Particle gradation curve of K1

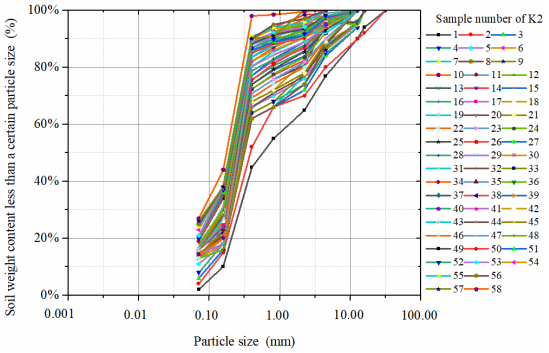

(b) Particle gradation curve of K2

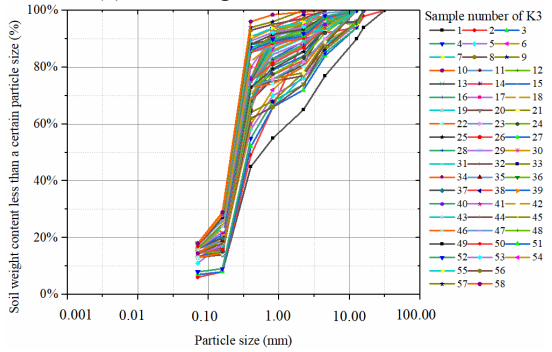

(c) Particle gradation curve of K3

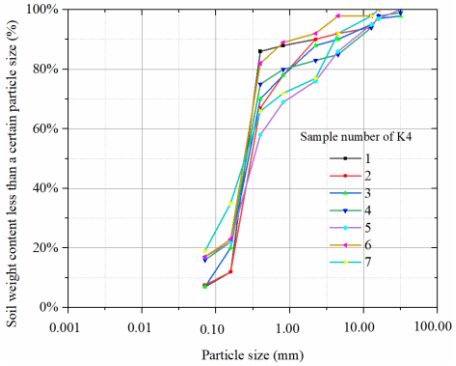

(d) Particle gradation curve of K4

Fig. 4 Particle gradation curve of Kurkar stratum

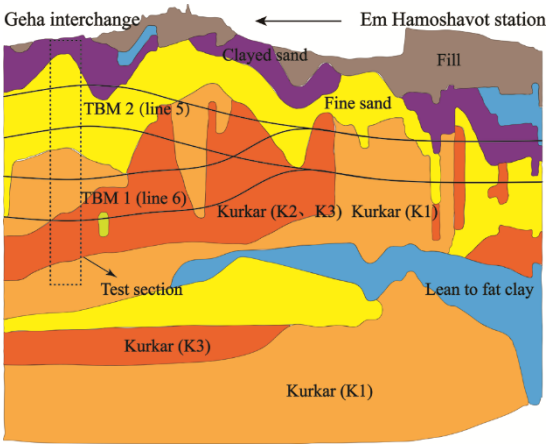

(a) Geological profile

(b) Geological field photographs: (I) K1, (II) K2, (III) K3, and (IV) fine sand

Fig. 5 Geological profile of monitoring section

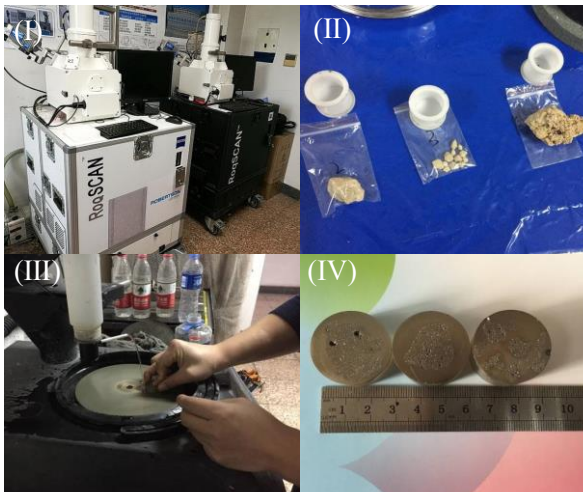

(a) Testing process: (I) Instrument, (II) samples of Kurkar, (III) sample preparation, and (IV) completed sample preparation

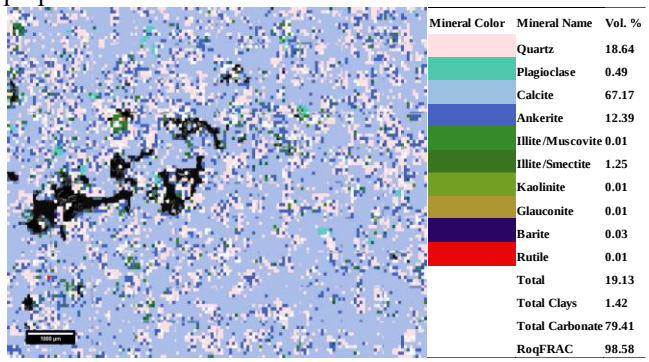

(b) Mineral composition of a sample

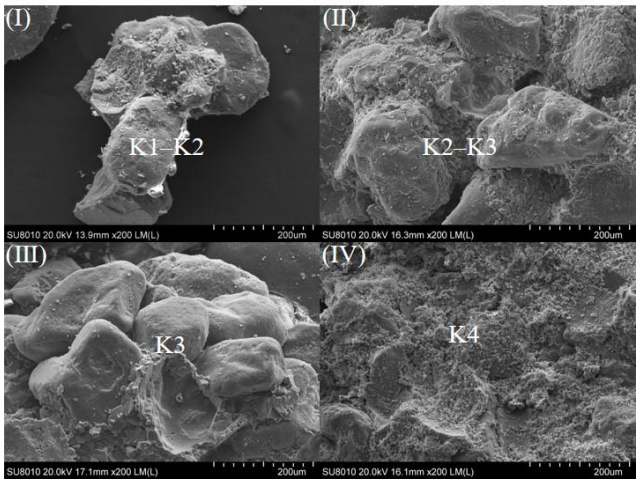

(c) Mineral microstructure of Kurkar sand

Fig. 6 Mineral composition test by RoqSCAN and mineral microstructure tested by scanning electron microscopy (SEM)

better roundness and more pits on the surface. The particles of K3 are mostly subangular to subcircular. Pores develop between the particles, and cement fills these pores. The macroscopic characteristics of K4 are pore development and calcite cement between quartz sand particles, as shown in Fig. 6(c).

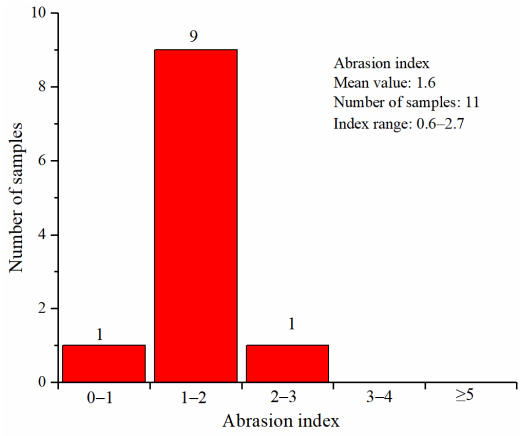

Fig. 7 Analysis chart of abrasion test

To evaluate the abrasiveness of the Kurkar stratum, the Cerchar abrasiveness test was performed on 11 Kurkar samples. The results demonstrated an abrasion index range of 0.6–2.7, with an average value of 1.6, as shown in Fig. 7. Therefore, Kurkar can be considered as a soil layer with certain abrasiveness. The unconfined compressive strengths of five well-cemented Kurkar specimens were tested, and the average was approximately 900 kN/m². Considering the geological factors, 19 double-edged hobs with a width of 43.18 cm each were arranged on the cutter head with a cutter spacing of 100 mm. The hobs can be replaced from the back of the cutter head. There are 120 cutters, 16 tearing knives, 16 edge scrapers, and 1 central fishtail knife.

3. Parameter studies

3.1 Overcut clearance of shield in curved section

The small turning radius of the shield will hinder its turning and cause overexcavation and shield jamming. The excavation diameter of the shield is 7,550 mm, the diameter and length of the front shield are 7,510 mm and 3,685 mm, respectively, and the diameter and length of the middle shield (including articulation joint) are 7,500 mm and 3,870 mm, respectively. The diameter and length of the tail shield (including the articulation joint) are 7,490 mm and 3,950 mm, respectively. To effectively solve the problem of shield tunneling in the case of a curve with a small radius, the shield articulation adopted a bilateral articulation design, as shown in Fig. 8. An active articulation was installed between the front and middle shields which had good directional performance and a large steering bending angle. The active articulation was placed in the front section of the shield, shortened the length of the shield body, and reduced the friction resistance of the soil and the load on the articulated jack. A passive articulation was installed between the middle and tail shields. Although the bending angle was small, the structure was simple and compact. In addition, the tail part of the shield can be towed.

As the shield advances in the curved section with a small turning radius, it may overexcavate the soil. Therefore,

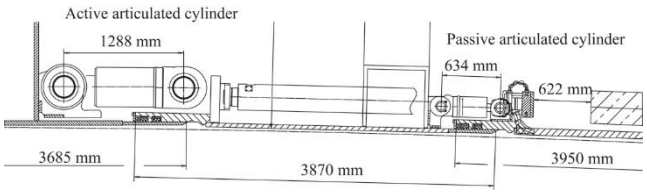

Fig. 8 Schematic of shield articulation

it is necessary to calculate and analyze the overexcavated volume of the shield. Fig. 9 illustrates the calculation of the overexcavation by the shield in the curved section. The following geometric relationships can be derived from the figure:

$$\delta = Od - D - OE, \tag{1}$$

$$Od^2 = (OE + D)^2 + \left(\frac{L}{2}\right)^2, \tag{2}$$

$$OF^2 = (OE + \frac{D}{2})^2 + \left(\frac{L}{2}\right)^2, \tag{3}$$

$$OF = R_0, \tag{4}$$

where D is the cutter head diameter, L is the shield length, δ is the shield overexcavation clearance, and O is the rotation center.

Substituting Eqs. (2)- (4) in Eq. (1) yields

$$\delta = \sqrt{\left(\sqrt{{R_0}^2 - \left(\frac{L}{2}\right)^2} + \frac{D}{2}\right)^2 + \left(\frac{L}{2}\right)^2} - \sqrt{{R_0}^2 - \left(\frac{L}{2}\right)^2} - \frac{D}{2} \tag{5}$$

where D = 7.55 m, L = 11.5 m, R_0 = 220 m, and the overexcavation clearance δ = 0.074 m.

The volume of the overexcavation clearance in the range of one ring segment of the curved section is

$$V_e = \frac{\pi}{4} l[(D + \delta)^2 - D^2] \tag{6}$$

where V_e is the volume of the overexcavation clearance, l is the segment width of the curved section, and l = 1.2 m and V_e = 1.058 m^3.

The theoretical excavation volume of each segment is

$$v = \left(\left(\frac{D}{2}\right)^2 - r^2\right)\pi l \tag{7}$$

where r is the outer radius of the tunnel (r = 3.6 m), and l is the segment's width. During the construction of the curved section, l = 1.2 m and v = 4.86 m^3. The sum of the theoretical volume of the curved section and the overexcavation soil volume is 5.918 m^3. In the linear section, l = 1.5 m, and the theoretical excavation volume is 6.079 m^3. The excavation volume of the curved section is basically equal to that of the linear section.

The theoretical grouting volume V_g of the curved section is

$$V_g = V_e + \frac{\pi}{4} l\left(D^2 - {D_0}^2\right), \tag{8}$$

where D_0 is the outer diameter of the tunnel (D_0 = 7.2 m).

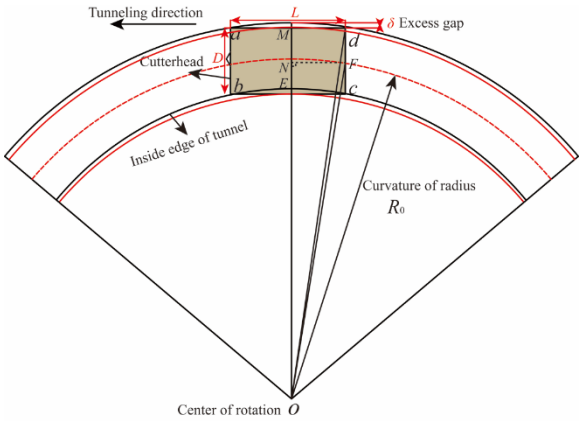

Fig. 9 Calculation of overexcavation volume caused by a small turning radius

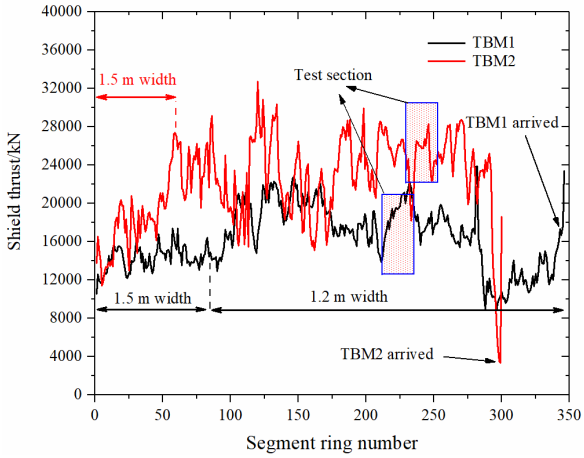

(a) Thrust comparison (TBM1)

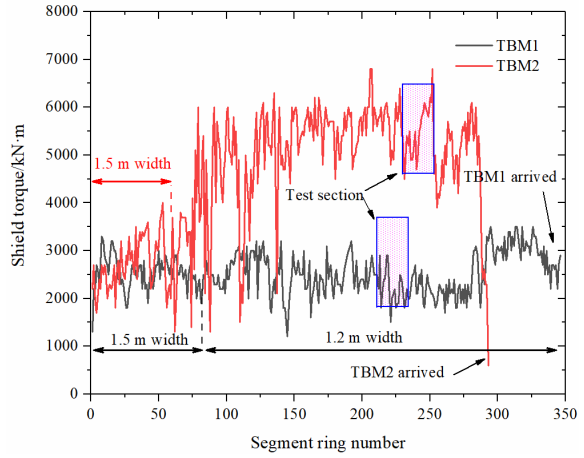

(b) Torque comparison (TBM2)

Fig. 10 Thrust and torque comparisons of TBM1 and TBM2

According to the calculation, V_g = 5.92 m^3.

3.2 Analysis of key tunneling parameters

3.2.1 Thrust and torque analysis

As observed in Fig. 5, TBM1 mainly passes through the Kurkar stratum, while TBM2 mainly passes through the fine-sand layer. A total of 346 and 299 rings were excavated

by TBM1 and TBM2, respectively. For TBM1, the thrust produced by the shield at a segment length of 1.5 m was less than that produced by the curved section at a segment length of 1.2 m, as shown in Fig. 10(a). The shield thrust in the linear section was 12,000–16,000 kN, and that in the curved section was 16,000–20,000 kN. The thrust produced by TBM2 was generally greater than that of TBM1 as it advanced through fine sand, as shown in Fig. 10(b). In the linear section, the thrust of the TBM2 was 16,000–20,000 kN. In the turning section, it was generally 24,000–28,000 kN. The torque of the shield in the down-track tunnel in the Kurkar stratum was 2,000–3,000 kN·m, and that in the up-track tunnel in fine sand was 5,000–6,000 kN·m. The shield of TBM2 had a rated torque of 5,265 kN·m, which was insufficient to propel the excavator through the fine-sand layer. In turn, this decelerated the machine. To solve this problem, two sets of driving motors were added following which the rated torque of the shield machine reached 6,435 kN·m and the breakout torque reached 9,331 kN·m. The torque of the shield machine improved to 5,000–6,000 kN·m, which in turn increased the tunneling speed. The up-track tunnel is in fine sand layer and the down-track tunnel is in the Kurkar layer. The fine sand is easily attached to the cutter head after soil improvement, resulting in greater thrust and torque of TBM2. The particle size of the Kurkar is larger than fine sand, so it is difficult to adhere to the cutter head, resulting in lesser thrust and torque of TBM1.

3.2.2 Analysis of earth pressure and excavated soil quantity

As shown in Fig. 11(a), as TBM1 advances in the Kurkar stratum, the earth pressure at the linear section of the shield is lower than that at the curved section. The tunneling face was relatively stable owing to the strength of the Kurkar stratum. The earth pressure in the upper soil chamber was 0.04–0.08 MPa, and that in the middle soil chamber was 0.08–0.12 MPa. Upon the arrival of the shield at the curved section, the earth pressure increased significantly to 0.1–0.14 MPa in the upper-soil chamber and 0.16–0.18 MPa in the middle-soil chamber. Approximately 30 rings before the shield arrived at the Geha interchange, the quantity of earth discharged from the soil chamber increased sharply and resulted in a drop in the earth's pressure. As observed in Fig. 11(b), the quantity of soil excavated by TBM2 in the Kurkar stratum varied considerably, which led to a large fluctuation in earth's pressure. The quantity of soil discharged by the screw conveyor in the sand layer remained stable. Therefore, the soil pressure remained stable at 0.07–0.09 MPa in the upper chamber and 0.1–0.12 MPa in the middle chamber. The quantity of soil discharged by the screw conveyor in Kurkar varied compared with those of the two shield machines. The discharged soil quantity in the fine-sand layer remained unchanged. The quantity of soil excavated by TBM1 in the linear section was approximately 90–100 tons, whereas that in the curved section was 80–100 tons. These outcomes indicate that overexcavation occurred during shield turning. As TBM2 advanced in the fine-sand layer, the quantity of soil excavated from the 1.2 m segment was basically equal to that from the 1.5 m segment. Therefore, a stable (yet with

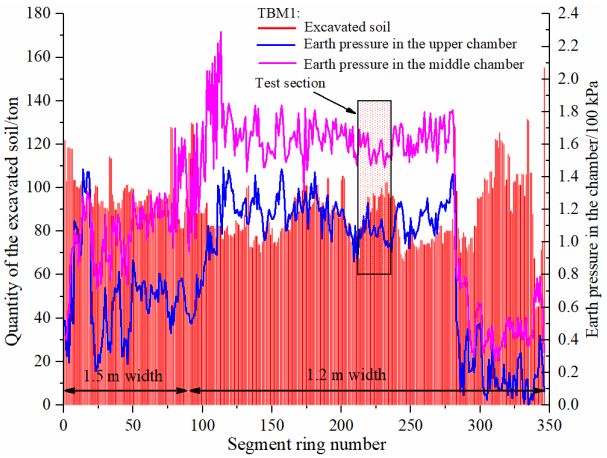

(a) TBM1

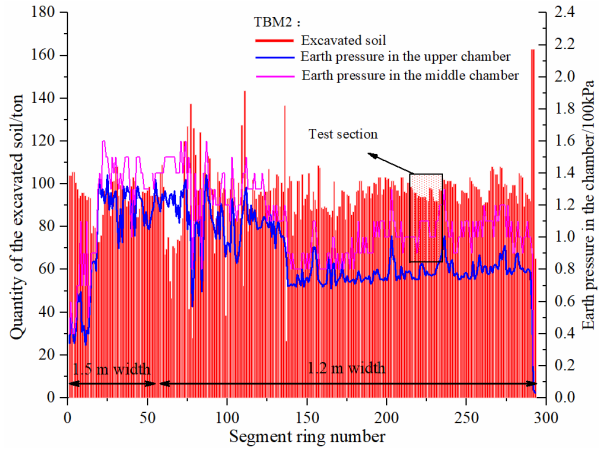

(b) TBM2

Fig. 11 Excavated soil volume and soil pressure of TBM1 and TBM2

an excess amount of) soil was excavated from the fine-sand layer. Although the quantity of soil excavated by TBM1 fluctuated considerably, its maximum value in the curved section was close to that in the linear section. This indicates that it was easy to inadvertently overexcavate the Kurkar stratum. As can be seen from the geological picture in Fig. 4, Kurkar is a weakly cemented calcareous sand layer. After disturbance of TBM cutter head, this type of cohesion is destroyed and the Kurkar becomes non-cohesive soil. The buried depth of TBM2 is greater than that of TBM1, so the face pressure of TBM2 is greater than that of TBM1.

3.2.3 Grouting pressure and grouting volume

The grouting pressure ranges of TBM1 and TBM2 were 0.2–0.3 MPa and 0.3–0.4 MPa, respectively, as shown in Fig. 12. The grouting pressure of TBM2 was greater than that of TBM1. However, the grouting volume of TBM1 was greater than that of TBM2, indicating that more grout had penetrated the Kurkar stratum. The grouting pressures of the linear and curved sections were basically the same, and the grouting volume of the linear section was higher than that of the curved one. In the Kurkar stratum, the amount of grout generated by TBM1 was 5–6 m^3. In the fine-sand layer, the grouting volume of TBM2 fluctuated considerably

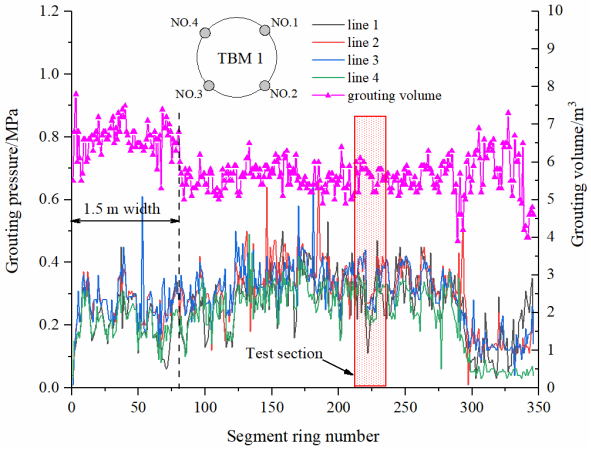

(a) TBM1

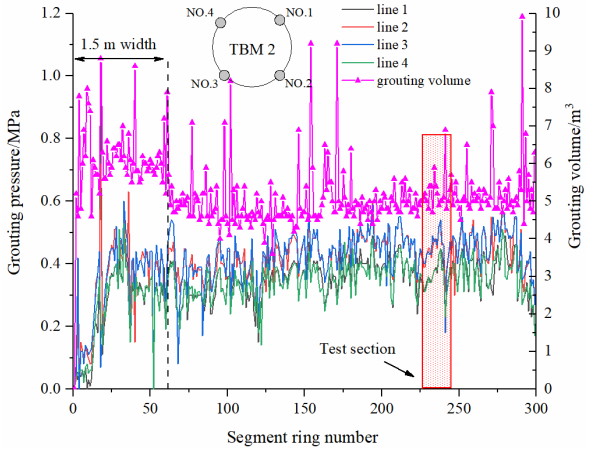

(b) TBM2

Fig. 12 Grouting pressure and grouting volume of TBM1 and TBM2

occasionally. This indicates that at certain grouting pressures, grout was easier to cause fine-sand cracks, which allowed more grout to enter the sand layer. Because shield tunneling may overexcavate the curved section, and frequent adjustment of shield attitude would increase the disturbance in the soil mass, synchronous grouting volume and grout quality should be strictly controlled in the curved section. In the construction process, the advancing speed of the excavator is matched with the grouting speed to ensure that the total amount of grout generated in each ring is adequate. The volume of the soil excavated outside the curve is greater than that inside it. Thus, the synchronized amount of grout outside the curve should be appropriately increased to prevent the segment dislocation attributed to the uneven extrusion of stratum stress. Generally, the grouting pressure of the down-track tunnel should be greater than that of the up-track tunnel. However, as can be seen in Fig. 12, the grouting amount of TBM2 fluctuates greatly, indicating that the soil of the up-track tunnel is easy to be split and destroyed by the grouting pressure. To ensure that the excavation gap of the up-track tunnel can be filled with grout, the grouting pressure of the TBM2 is made greater than that of the TBM1. Another reason for the high grouting pressure of TBM2 is to uplift the soil to a certain extent and reduce the surface settlement.

Table 3 Statistics of tunneling speed interval

Construction days (day)	1–5	6–10	11–15	16–20	21–25
Speed interval (mm/min)	37–60	29–33	25–43	28–34	21–43
	40–64	22–35	29–46	24–32	17–48
	36–50	25–30	32–41	26–31	24–40
	31–38	25–31	26–37	30–36	24–32
	23–50	22–30	21–34	15–37	20–60

3.2.4 Fuzzy statistical analysis of tunneling speed

To explore the normal operating state of the two shield machines in the curved section with a small turning radius, the tunneling speeds of TBM1 and TBM2 were statistically analyzed. The tunneling speeds of TBM1 (in rings 82–346) and TBM2 (in rings 60–299) were selected for the analysis. The statistical value of the tunneling speed is the average tunneling speed of each ring. Anomalous tunneling speeds caused by shield machine failure were eliminated from the analysis. The fuzzy statistical test was carried out for the construction records of shield tunneling in this area, according to the fuzzy set theory, and the normal driving speed of shield tunneling was obtained. The concept of fuzzy theory was first proposed by Zadeh (1968) to express uncertainty of things. Determining convergence frequency A(x) is primary task to deal with fuzzy phenomenon in practical applications. In this study, the convergence frequency can be calculated by the following formula (Zheng *et al*. 2015)

$$A(v) = m/n$$

where v is the recorded shield advance speed, m is the number of days recording a specified v, and n is the total number of construction days. First, the construction days of TBM1 and TBM2 were set to 25 and 35 days, respectively. The detailed statistical analysis uses the tunneling speed of TBM1 as the sample. According to the statistics of the daily minimum and maximum tunneling speeds, 25 groups of speed intervals were obtained, as listed in Table 3.

According to the sample, the minimum data value was 15 mm/min, and the maximum value was 64 mm/min. Therefore, taking 14.5 mm/min as the starting point, 64.5 mm/min as the end point, and 1 mm/min as the interval length, the “universe” in the fuzzy set was divided into 50 intervals, and each interval was represented by the median value to calculate the membership frequency. Considering the shield tunneling speed interval as the abscissa and the convergence frequency as the ordinate, a histogram of the convergence frequency is drawn in Fig. 13. The histogram is fitted to obtain the Gaussian distribution curve of the speed, and the fitting distribution curve is given by Eq. (9). According to the fitting curve, the speed convergence frequency of the shield conforms to the Gaussian distribution. The same method was used for the statistical analysis of TBM2, as shown in Fig. 13(b), and the fitting distribution curve is given by Eq. (10). According to the speed convergence frequency histogram, the tunneling speed of TBM1 is concentrated in the range of 28–32

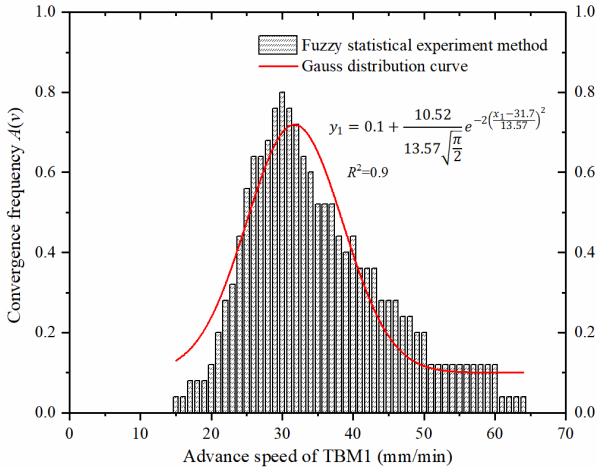

(a) TBM1

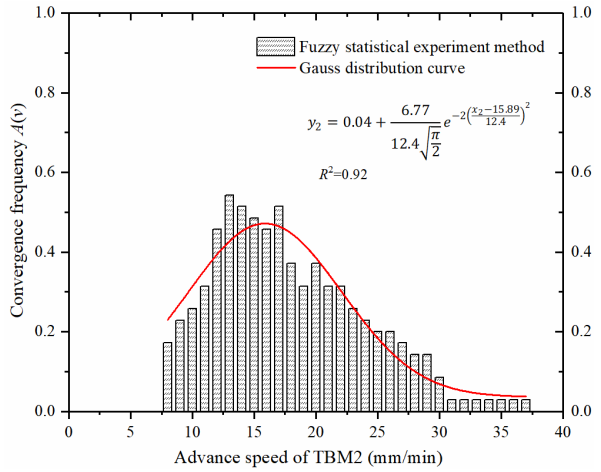

(b) TBM2

Fig. 13 Histogram of frequency and fitting curve of shield tunneling speed

mm/min, whereas that of TBM2 is concentrated in the range of 13–17 mm/min. Therefore, the tunneling speed of TBM1 in the Kurkar stratum is equal to two times that of TBM2 in the sand layer.

4. Results and discussion

4.1 Subsurface vertical displacements from rod extensometers

When the shield excavated the down-track tunnel, TBM1 passed through extensometers E1, E2, and E3 in sequence. E1 was located on the right side of the shield tunneling direction, 3 m from the right-most tunnel edge. Figs. 14(a) and 14(b) show the settlement values of extensometer E1 at different depths. The maximum settlement of the anchor with a buried depth of 27.5 m was approximately 10 mm. The anchor was located within the tunnel excavation diameter. The settlement of the anchor was located at the upper part of the tunnel with a buried depth of 20 m and was approximately 7 mm. Additionally, the settlement of the upper part of the tunnel, with a buried depth of 13 m, was approximately 2.5 mm. The anchor, with a depth of 5 m, exhibited a subtle uplift of approximately 1.5 mm. Interestingly, the anchor with a depth of 36 m below the tunnel rose gradually when the shield arrived. After the tail shield passed, the anchor began to sink again owing to the influence of the tail-skin grouting pressure. As the buried depth decreased, the settlement gradually decreased. Extensometer E2 was positioned between the two tunnels. The measurement points of all the three anchors showed a significant upward displacement when TBM1 and TBM2 passed beneath E2, as shown in Figs. 14(c) and 14(d). There was an uplift of approximately 2.2 mm in the anchor with a depth of 7 m, 1.7 mm in the anchor with a depth of 5 m, and 0.6 mm in the anchor with a depth of 3 m. As the distance between E3 and the first tunnel was longer than E1, the settlement values of each point were less than E1, as shown in Figs. 14(e) and 14(f). The settlement value of the anchor with a buried depth of 27.5 m was 4 mm. As the anchor depth decreased, the settlement value gradually decreased, but there was no obvious settlement or uplift on the surface. When TBM2 excavated the up-track tunnel, E1, E2, and E3 did not exhibit extensive settlements. This may be attributed to the high thrust of the shield. The three anchors of E2 were located in the upper part of the tunnel; thus, the monitoring value of each anchor showed an uplift. For E1 and E3, the anchors at the upper part of the tunnel showed a settlement of 0.2–0.5 mm; the anchors at the lower part of the tunnel showed an uplift of 0.5–1 mm. The anchor with a depth of 36 m was hardly affected by the excavation of the up-track tunnel. By comparing the vertical displacements of the stratum caused by the up-track and down-track tunnels, it can be seen that the settlements caused by the down-track tunnel is greater than that caused by the up-track tunnel, because the thrust, torque and grouting pressure of the shield of the down-track tunnel are smaller than that of the up-track tunnel. The settlement caused by the construction of the down-track tunnel increases with the increase of buried depth, while the soil displacement caused by the construction of the up-track tunnel first uplifts and then sinks.

4.2 Ground surface settlement

Measurement curves N1–N3 in Fig. 15(a) show the relationships between the cutter head position of TBM1 and surface settlement. N1 and N3 were located at the center of the tunnel axis, whereas N2 was located approximately 3 m from the edge of the tunnel. Curves N1 and N3 show that when the cutter head of the shield was 10 m in front of the measuring point, the ground surface begins to rise gradually. N2, however, shows that the settlement is slow. During the period between the arrival of the shield cutter head at the monitoring point to the departure of the tail shield from that point, the surface deformation revealed an abrupt settlement of 3–5 mm. The effect of synchronous grouting was obvious. The uplift value under the influence of grouting was approximately 2–4 mm. After grouting stopped, the surface subsidence was approximately 1–3 mm. In general, the settlement at the tunnel axis was

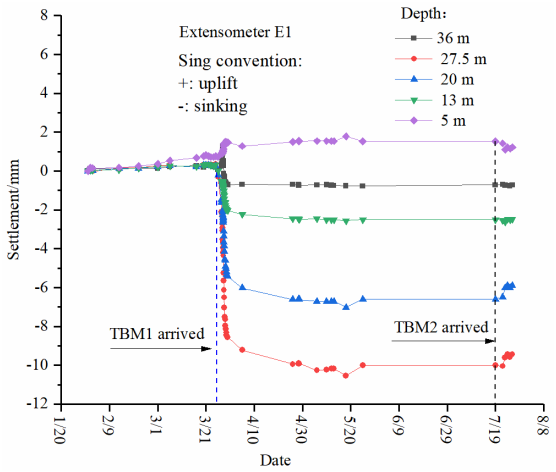

(a) Total settlement of E1

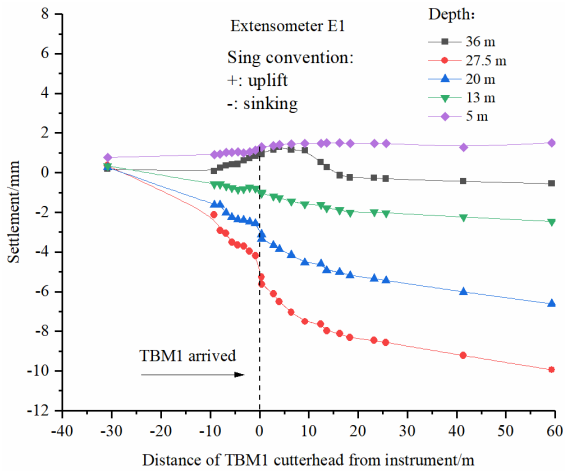

(b) Settlement of E1 caused by TBM1

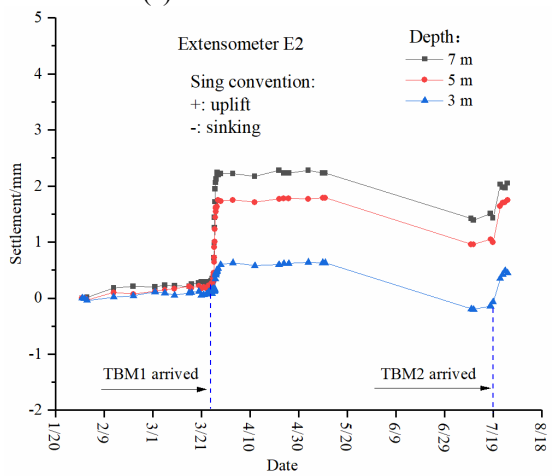

(c) Total settlement of E2

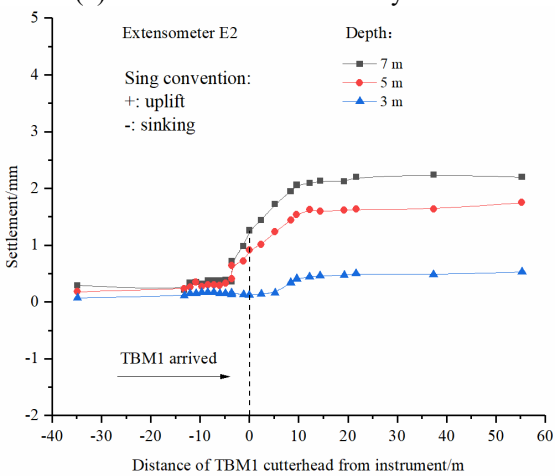

(d) Settlement of E2 caused by TBM1

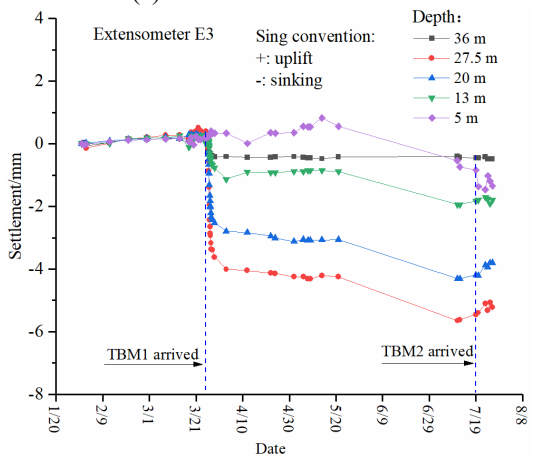

(e) Total settlement of E3

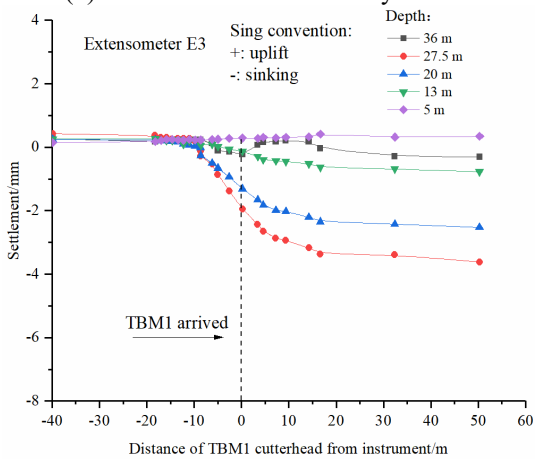

(f) Settlement of E3 caused by TBM1

Fig. 14 Subsurface vertical soil displacements at different depths

approximately 3–4 mm, whereas the settlement at the edge was approximately 0.5–1 mm. The tail shield was approximately 30 m from the measurement point for secondary grouting. However, the effect of secondary grouting was not apparent. When TBM2 passed through the monitoring section, the three measurement points at the edge of the tunnel showed an obvious uplift of 1–2 mm, as shown in Fig. 15(b). After the shield passed, the ground began to sink, and the settlement value was approximately 2–3 mm. Synchronous grouting only caused a subtle uplift of approximately 0.5 mm. As the buried depth of the down-track tunnel is larger than that of the up-track tunnel, it can be seen from the surface settlement that the settlement caused by the down-track tunnel has no obvious uplift before the arrival of the shield, while the up-track tunnel first uplifts and then sinks. The grouting pressure can prevent the aggravation of surface settlement, which will produce slight uplift.

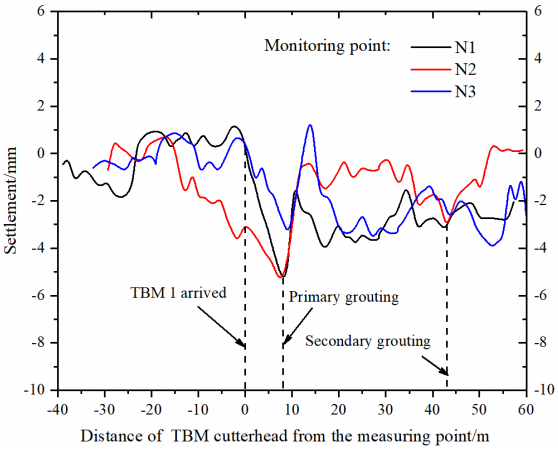

(a) Surface subsidence caused by TBM1

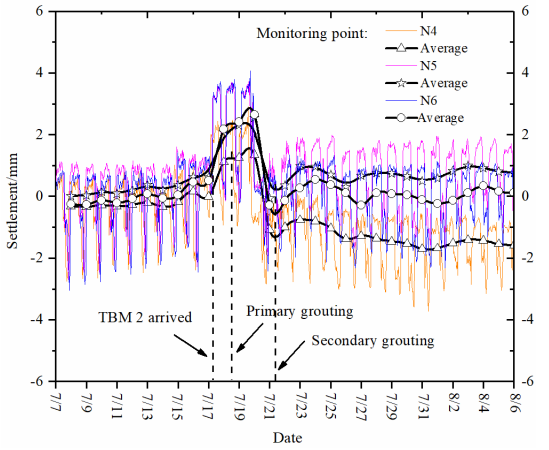

(b) Surface subsidence caused by TBM2

Fig. 15 Surface subsidence

4.2 Ground surface settlement

Measurement curves N1–N3 in Fig. 15(a) show the relationships between the cutter head position of TBM1 and surface settlement. N1 and N3 were located at the center of the tunnel axis, whereas N2 was located approximately 3 m from the edge of the tunnel. Curves N1 and N3 show that when the cutter head of the shield was 10 m in front of the measuring point, the ground surface begins to rise gradually. N2, however, shows that the settlement is slow. During the period between the arrival of the shield cutter head at the monitoring point to the departure of the tail shield from that point, the surface deformation revealed an abrupt settlement of 3–5 mm. The effect of synchronous grouting was obvious. The uplift value under the influence of grouting was approximately 2–4 mm. After grouting stopped, the surface subsidence was approximately 1–3 mm. In general, the settlement at the tunnel axis was approximately 3–4 mm, whereas the settlement at the edge was approximately 0.5–1 mm. The tail shield was approximately 30 m from the measurement point for secondary grouting. However, the effect of secondary grouting was not apparent. When TBM2 passed through the monitoring section, the three measurement points at the edge of the tunnel showed an obvious uplift of 1–2 mm, as shown in Fig. 15(b). After the shield passed, the ground began to sink, and the settlement value was approximately 2–3 mm. Synchronous grouting only caused a subtle uplift of approximately 0.5 mm. As the buried depth of the down-track tunnel is larger than that of the up-track tunnel, it can be seen from the surface settlement that the settlement caused by the down-track tunnel has no obvious uplift before the arrival of the shield, while the up-track tunnel first uplifts and then sinks. The grouting pressure can prevent the aggravation of surface settlement, which will produce slight uplift.

4.3 Subsurface horizontal displacements

The inclinometers monitored the transverse horizontal displacement of the soil perpendicular to the tunnel and the longitudinal horizontal displacement of the soil parallel to the tunnel. In the direction of motion, as TBM1 passes through C1, the soil movement at the excavation scope of the tunnel was the largest, and the movement of the upper part was greater than that of the lower part because of the depth of the tunnel (Fig. 16(a)). As the cutter head approached the inclinometer, the soil moved from its location away from the excavation face toward the excavation face. The longitudinal horizontal displacement within the excavation range was approximately 10 mm. In the direction perpendicular to the tunnel, the soil at the bottom of the tunnel moved from a location near the tunnel to another location farther away from it, and the soil at the top of the tunnel moved from a location farther from the tunnel. The displacement variation was within 8 mm, as shown in Fig. 16(b). As TBM2 passed through C1, the soil moved toward the excavation face from a place farther from it. However, after the tail shield passed C1, the soil had a rebound of 3–6 mm, as shown in Figs. 16(c)–(d). Owing to the shallowness of the tunnel in the upper part, the horizontal displacement of the soil mass in that part was greater than in the excavation scope of the tunnel. As the depth increased, the influence of the shield excavation on the horizontal displacement of soil became weaker.

When TBM1 passed through C2, no obvious displacement in the excavation range was observed, but a large deformation occurred at the bottom of the tunnel, as shown in Figs. 17(a) and 17(b). The reason for this displacement may be related to the stratum. The soil within the excavation scope belonged to the Kurkar K2 stratum, which has a certain cementation and strength. The soil at the bottom was loose, which is why the displacement was large. When TBM2 passed through C2, the deformation of the soil was similar to that when TBM2 passed through C1. With an increase in the buried depth of the inclinometer, soil displacement decreased, as shown in Figs. 17(c) and 17(d). It can be seen from in Figs. 16 and 17 that the transverse displacements caused by the excavation of the do wn-track tunnel by TBM1 are significantly smaller than those caused by the excavation of the up-track tunnel by TBM2. The reason for this is that TBM1 excavated weakly cemented Kurkar stratum, while TBM2 excavated fine sand stratum, and the soil stiffness of Kurkar stratum is higher than that of sand stratum. Therefore, it is noteworthy that the excavation of the up-track tunnel may have a great impact on the adjacent pipelines.

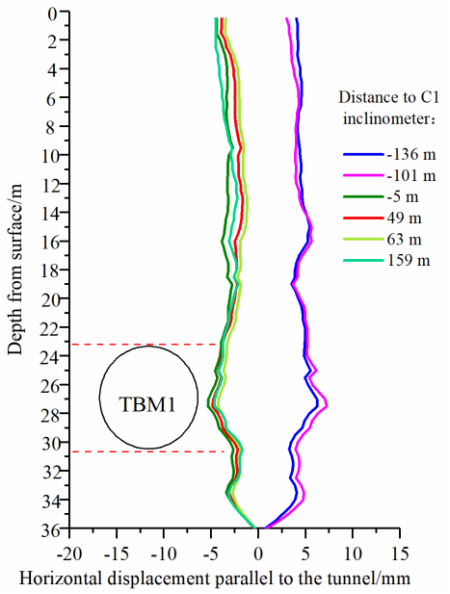

(a) Longitudinal displacement induced by TBM1

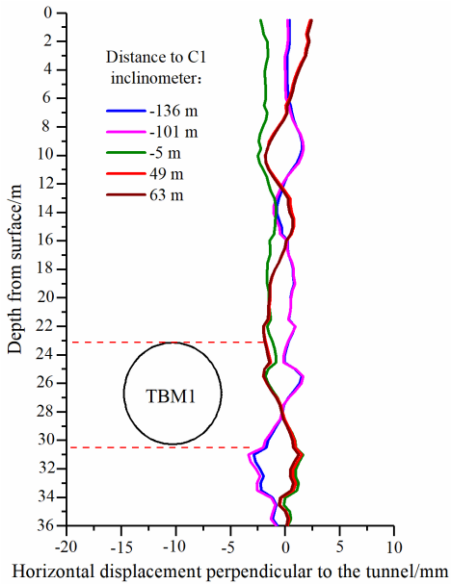

(b) Transverse displacement induced by TBM1

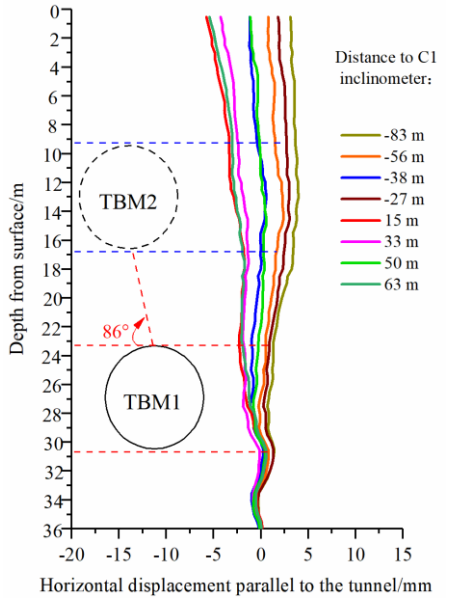

(c) Longitudinal displacement induced by TBM2

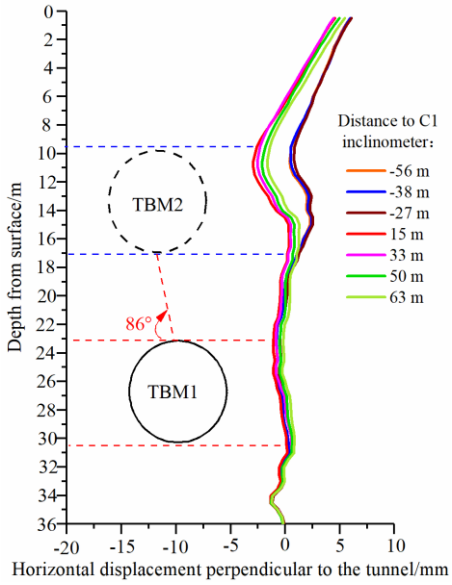

(d) Transverse displacement induced by TBM2

Fig. 16 Results from inclinometer C1

4.4 Lining response

The lining response was monitored from three directions (X, Y, and Z). When the shield reached the monitoring section from the vertical direction Z, the segments sank first, and the settlement value was approximately 0.2–0.3 mm, as shown in Fig. 18(a). After the rear of the shield passed through the segments, the segments began to gradually float upward, owing to the stress relief of the tunnel excavation. The uplift value was approximately 0.5 mm. The segment eventually subsided, the final settlement value exceeded the uplift value, and the entire segment exhibited settlement. From the X direction, the monitoring points P1 and P3 showed that the segment followed a trend of eastward movement, and the P2 monitoring point showed that the segment moved westward, as shown in Fig. 18(b). Thus, the integral segment has a flattened shape. P2 had the largest displacement, which was approximately 1 mm to the west. This may be attributed to the fact that as the shield turned, the articulation of the shield required continuous adjustment. This cut the soil toward the center of the turning radius and caused it to squeeze inward. P1 and P3 show that when the shield reached the monitoring section from the Y direction, the shield moved toward the south by approximately 0.2 mm. P2 shows that the shield moved to the north by approximately 1 mm. Thus, the entire ring segment underwent compression deformation. Under the influence of the construction load of the up-tack tunnel, the segments of the down-track tunnel first move downward, and then float upward after the soil is unloaded. The two sides of the tunnel arch also tend to move outward slightly, which may lead to the elliptical deformation of the tunnel.

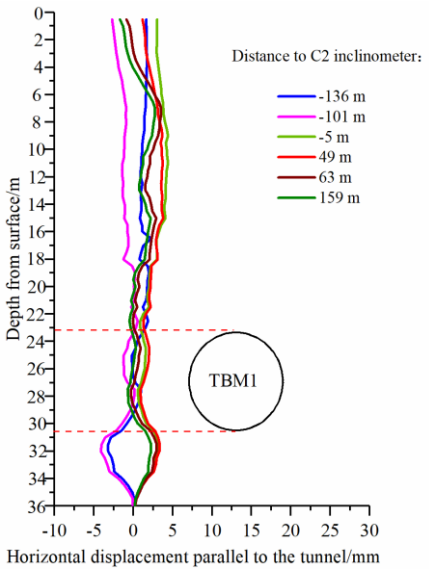

(a) Longitudinal displacement induced by TBM1

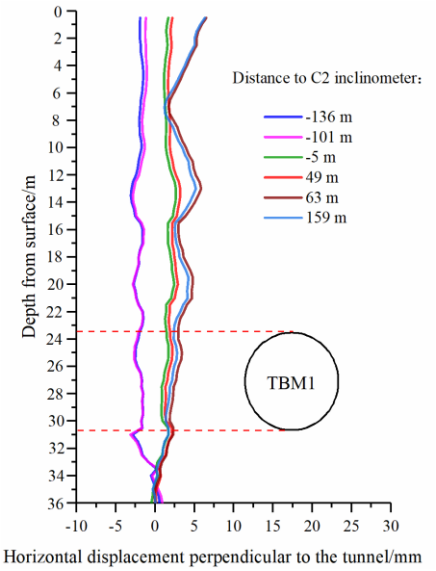

(b) Transverse displacement induced by TBM1

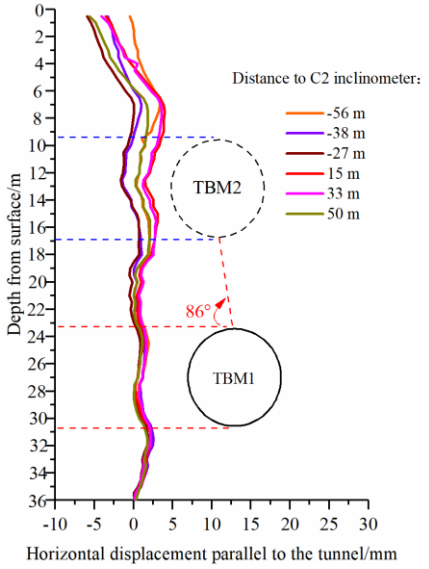

(c) Longitudinal displacement induced by TBM2

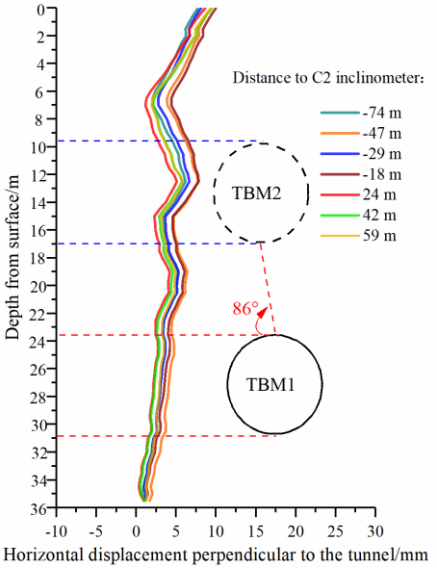

(d) Transverse displacement induced by TBM2

Fig. 17 Results from inclinometer C2

5. Conclusions

Short-term underground and surface ground responses due to overlapping shield tunnels were analyzed by combining the geological characteristics of the stratum and shield parameters with a small turning radius. The eastern section of the Tel Aviv Red Line light rail was chosen as the study area. The following conclusions were drawn:

1. Owing to the effect of the turning radius, the thrust and torque of the shield machine in the curved section were larger than those in the linear section. The required thrust and torque in the fine-sand layer were greater than those in the Kurkar stratum. The theoretical calculation shows that the volume of soil excavated by the shield in the curved section is close to that in the linear section. Compared with the monitoring results of the real-time weighing equipment of the *in situ* belt conveyor used to transport the soil, the theoretical results revealed over-excavation in the curved section. The amount of over-excavation in the fine-sand layer was greater than that in the Kurkar stratum.
2. The grouting pressure of the shield in the fine-sand layer was marginally higher than that in the Kurkar stratum, but neither fluctuated significantly. In the fine-sand layer, the sudden increase in the grouting volume was more frequent than that in the Kurkar stratum, indicating that under the existing grouting pressure, synchronous grouting in the fine-sand stratum will more likely cause splitting failure of the soil mass.
3. Based on the fuzzy statistical analysis of speed, the convergence frequencyof the shield tunneling speed was in accordance with Gaussian curve fitting. The tunneling speed of the down-track tunnel in the Kurkar stratum varied from 27 to 32 mm/min, while that of the up-track tunnel varied from 13 to 17 mm/min in the fine-sand layer. The construction speed of the down-track tunnel was approximately equal to twice that of the up-track tunnel.

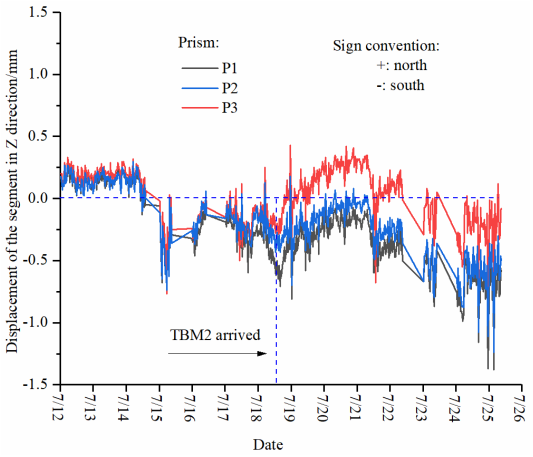

(a) Deformation in Z direction

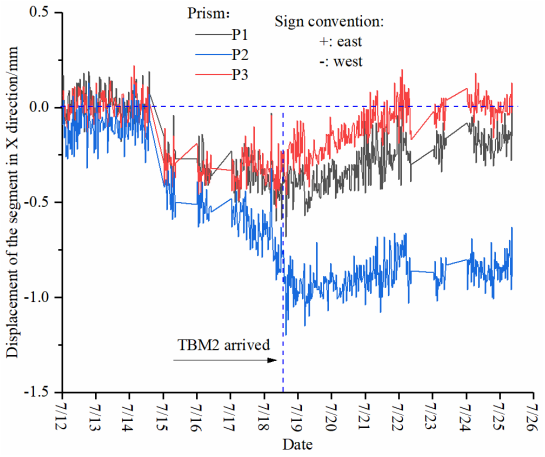

(b) Deformation in X direction

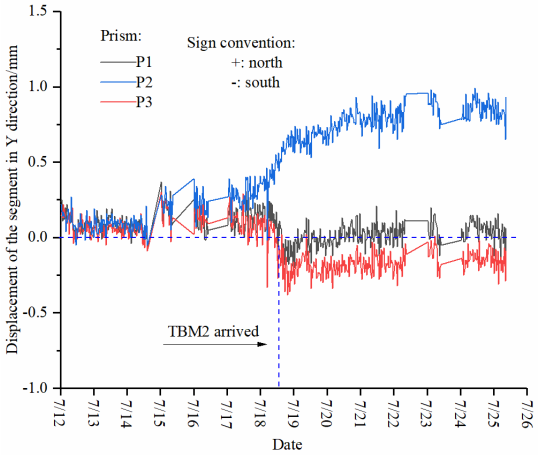

(c) Deformation in Y direction

Fig. 18 Displacements of segments

4. Before the shield cutter head arrived, the soil displacement increased in a direction away from the tunnel. After the shield cutter head had passed, the soil deformed toward the tunnel. The transverse horizontal displacement caused by the excavation of the up-track tunnel was generally greater than that of the down-track tunnel, thus indicating that the transverse horizontal displacement of the fine-sand layer was greater than that of the Kurkar stratum. In terms of the excavation of the down-track tunnel, the transverse deformation of the bottom and the top of the up-track tunnel were greater than those of the Kurkar stratum. As the shield advanced, the soil moved toward the direction of shield tunneling subject to the influence of thrust. As the shield gradually approached and passed through the inclinometer, the soil rebounded and moved to the rear of the shield. The excavation of the down-track tunnel strongly influenced the transverse displacement of the soil in the up-track tunnel, while the excavation of the up-track tunnel had a minor influence on the soil in the down-track tunnel.

5. For the vertical displacement of the deep soil, the closer the shield was to the tunnel excavation range, the greater the soil settlement. The settlement of the soil gradually decreased as the buried depth decreased, and the ground surface was affected by the thrust of the shield, which resulted in an uplift. For the segment deformation, after the shield reached the monitoring section, segment settlement was approximately 0.5–1 mm. After the shield passed, the unloading of the excavated soil caused the segment to rebound by approximately 0.5 mm. The entire ring segment underwent compression deformation.

The surface settlement caused by the construction of overlapping twin shield tunnel is different from that of parallel tunnel construction. In order to control the surface settlement caused by the construction of two tunnels, it is necessary to strictly control various construction parameters and clarify the causes of the settlement. The lateral displacement caused by excavation in Kurkar stratum is less than that in fine sand stratum. In order to prevent the disturbance caused by the construction of the second tunnel from aggravating the surface settlement, the parameters of the up-track tunnel construction can be improved.

Acknowledgments

The research described in this paper was financially supported by the National Natural Science Foundation of China (Grant No. U1261212). We also thank the NTA-Metropolitan Mass Transit System Ltd., China Civil Engineering Construction Corporation, Danya JV Ltd., and

WBI Ltd. for providing full access to the project material and test data of the eastern section Red Line light rail project.

References

Attewell, P.B. and Woodman, J.P. (1982), "Predicting the dynamics of ground settlement and its derivatives caused by tunnelling in soil", *Ground Eng.*, **15**(8), 9-6.

Broere, W. and Festa, D. (2017), "Correlation between the kinematics of a tunnel boring machine and the observed soil displacements", *Tunn. Undergr. Sp. Tech.*, **70**, 125-147. https://doi.org/10.1016/j.tust.2017.07.014.

Celestino, T.B., Gomes, R.A.M.P. and Bortolucci, A.A. (2000), "Errors in ground distortions due to settlement trough adjustment," *Tunn. Undergr. Sp. Tech.,* **15**, 97-100. https://doi.org/10.1016/S0886-7798(99)00054-1.

Dias, D. and Kastner, R. (2013), "Movements caused by the excavation of tunnels using face pressurized shields -Analysis of monitoring and numerical modeling results", *Eng. Geol.*, **152**, 17-25. https://doi.org/10.1016/j.enggeo.2012.10.002.

Ding, Z., Wei, X.J. and Wei, G. (2017), "Prediction methods on tunnel-excavation induced surface settlement around adjacent building", *Geomech. Eng.*, **12**(2), 185-195. https://doi.org/10.12989/gae.2017.12.2.185.

Eskandari, F., Goharrizi, K.G. and Hooti, A. (2018), "The impact of EPB pressure on surface settlement and face displacement in intersection of triplet tunnels at Mashhad metro", *Geomech. Eng.*, **15**(2), 769-774. https://doi.org/10.12989/gae.2018.15.2.769.

Fang, K., Yang, Z., Jiang, Y., Sun, Z. and Wang, Z. (2020), "Surface subsidence characteristics of fully overlapping tunnels constructed using tunnel boring machine in a clay stratum", *Comput. Geotech*., **125**, 103679. https://doi.org/10.1016/j.compgeo.2020.103679.

Festa, D., Broere, W. and Bosch, J.W. (2015), "Kinematic behaviour of a tunnel boring machine in soft soil: Theory and observations", *Tunn. Undergr*. *Sp. Tech.*, **49**, 208–217. https://doi.org/10.1016/j.tust.2015.03.007.

Frydman, S. (2011), "Characterizing the geotechnical properties of natural, Israeli, partially cemented sands", *Geomech. Eng*., **3**(4), 323-337. https://doi.org/10.12989/gae.2011.3.4.323.

Hasanpour, R., Chakeri, H., Ozcelik, Y. and Denek, H. (2012), "Evaluation of surface settlements in the Istanbul metro in terms of analytical, numerical and direct measurements", *Bull. Eng. Geol. Environ.*, **71**, 499-510. https://doi.org/10.1007/s10064-012-0428-5.

Karakus, M., Ozsan, A. and Basarir, H. (2007), "Finite element analysis for the twin metro tunnel constructed in Ankara Clay, Turkey", *Bull. Eng. Geol. Environ*., **66**, 71-–79. https://doi.org/10.1007/s10064-006-0056-z.

Kim, D., Pham, K., Park, S., Oh, J.Y. and Hangseok, C. (2020), "Determination of effective parameters on surface settlement during shield TBM", *Geomech. Eng.*, **21**(2), 153-164. https://doi.org/10.12989/gae.2020.21.2.153.

Kim, K., Oh, J., Lee, H., Kim, D. and Choi, H. (2018), "Critical face pressure and backfill pressure in shield TBM tunneling on soft ground", *Geomech. Eng.*, **15**(3), 823-831. https://doi.org/10.12989/gae.2018.15.3.823.

Liu, B., Yu, Z.W., Hang, Y.H., Wang, Z.L., Yang, S. and Liu, H. (2020), "A simplified combined analytical method for evaluating the effect of deep surface excavations on the shield metro tunnels", *Geomech. Eng.*, **23**(5), 405-418. https://doi.org/10.12989/gae.2020.23.5.405.

Loganathan, N. and Poulos, H.G. (1998), "Analytical prediction for tunneling-induced ground movements in clays", *J. Geotech. Geoenviron. Eng.* **124**, 846-856. https://doi.org/10.1061/(ASCE)1090-0241(1998)124:9(846).

Mair, R.J., Taylor, R.N. and Bracegirdle, A. (1993), "Subsurface settlement profiles above tunnels in clays", *Géotechnique*, **43**, 315-320. https://doi.org/10.1680/geot.1993.43.2.315.

Melis, M., Medina, L. and Rodriguez, J.M. (2002), "Prediction and analysis of subsidence induced by shield tunnelling in the Madrid metro extension", *Can. Geotech. J.*, **39**, 1273-1287. https://doi.org/10.1139/t02-073.

Miliziano, S. and de Lillis, A. (2019), "Predicted and observed settlements induced by the mechanized tunnel excavation of metro line C near S Giovanni station in Rome", *Tunn. Undergr. Sp. Tech.*, **86**, 236–246. https://doi.org/10.1016/j.tust.2019.01.022.

Mollon, G., Dias, D. and Soubra, A.H. (2013), "Probabilistic analyses of tunneling-induced ground movements", *Acta Geotech.* **8**, 181-199. https://doi.org/10.1007/s11440-012-0182-7.

Nawel, B. and Salah, M. (2015), "Numerical modeling of two parallel tunnels interaction using three-dimensional finite elements method", *Geomech. Eng.*, **9**(6), 775-791. https://doi.org/10.12989/gae.2015.9.6.775.

Nelson, J.T. and Watry, D.L. (2015), *Vibration Control at Sound Transit*, Springer, Berlin, Heidelberg, Germany, 313-320.

O'Reilly, M.P. and New, B.M. (1982), "Settlements above tunnels in the United Kingdom – Their magnitude and prediction", *Proc. Tunn.*, IMM, London, 173-181.

Ocak, I. (2013), "Interaction of longitudinal surface settlements for twin tunnels in shallow and soft soils: The case of Istanbul Metro", *Environ. Earth. Sci.,* **69**, 1673-1683. https://doi.org/10.1007/s12665-012-2002-7.

Peck, R.B. (1969), "Deep excavations and tunneling in soft ground", *Proceedings of the 7th International Conference on Soil Mechanics and Foundation Engineering*, Mexico City, Mexico.

Qi, W.Q., Yang, Z.Y., Jiang, Y.S., Shao, X.K. and Yang. X. (2021), "Structural Deformation of Existing Horseshoe-Shaped Tunnels by Shield Overcrossing", *KSCE J. Civ. Eng*., **25**(2), 735-749. https://doi.org/10.1007/s12205-020-0599-8.

Rezaei, A.H., Shirzehhagh, M. and Golpasand, M.R.B. (2019), "EPB tunneling in cohesionless soils: A study on Tabriz Metro settlements", *Geomech. Eng.*, **19**(2), 153-165. https://doi.org/10.12989/gae.2019.19.2.153.

Rowe, R.K. and Lee, K.M. (1992), "Subsidence owing to tunnelling II: Evaluation of a prediction technique", *Can. Geotech. J.*, **29**, 941-954. https://doi.org/10.1139/t92-105.

Standing, J.R. and Selemetas, J.R. (2013), "Greenfield ground response to EPBM tunnelling in London Clay", *Gëotechnique* **63**(12), 989-1007. https://doi.org/10.1680/geot.12.P.154.

Sugimoto, M., Sramoon, A., Konishi, S. and Sato, Y. (2007), "Simulation of shield tunneling behavior along a curved alignment in a multilayered ground", *J. Geotech. Geoenviron. Eng.*, **133**(6), 684-694. https://doi.org/10.1061/(ASCE)1090-0241(2007)133:6(684).

Sugiyama, T., Hagiwara, T., Nomoto, T., Ano, Y., Mair, R.J., Bolton, M.D. and Soga, K. (1999), "Observations of ground movements during tunnel construction by slurry shield method at the docklands light railway Lewisham extension-East London", *Soils Found*., **39**(3), 99-112. https://doi.org/10.3208/sandf.39.3_99.

Verruijt, A. and Booker, J.R. (1996), "Surface settlements due to deformation of a tunnel in an elastic half plane", *Géotechnique*, **46**(4), 753-756. https://doi.org/10.1680/geot.1996.46.4.753.

Wan, M.S.P., Standing, J.R., Potts, D.M. and Burland, J.B. (2017), "Measured short-term ground surface response to EPBM tunnelling in London clay", *Géotechnique*, **67**(5), 420–445.

https://doi.org/10.1680/jgeot.16.P.099.
Yamaguchi, I., Yamazaki, I. and Kiritani, Y. (1998), "Study of ground-tunnel interactions of four shield tunnels driven in close proximity, in relation to design and construction of parallel shield tunnels", *Tunn. Undergr. Sp. Tech.*, **13**(3), 289–304. https://doi.org/10.1016/S0886-7798(98)00063-7.
Zadeh, L.A. (1968), "Probability measures of fuzzy events", *J. Math. Anal. Appl.*, **23**(2), 421-427. https://doi.org/10.1016/0022-247x(68)90078-4.
Zheng, G., Lu, P. and Diao, Y. (2015), "Advance speed-based parametric study of greenfield deformation induced by EPBM tunneling in soft ground", *Comput. Geotech*., **65**, 220-232. https://doi.org/10.1016/j.compgeo.2014.12.013.

GC